Journal of Organometallic Chemistry 897 (2019) 170–177

Contents lists available at ScienceDirect

Journal of Organometallic Chemistry

journal homepage: www.elsevier.com/locate/jorganchem

Supramolecular assemblies and photophysical properties of ionic homo- and heteronuclear metallophilic complexes

Noora Svahn [a], Ingrid Sanz [a], Kari Rissanen [b], Laura Rodríguez [a, c, *]

[a] Departament de Química Inorgànica i Orgànica, Secció de Química Inorgànica, Universitat de Barcelona, Martí i Franquès 1-11, 08028, Barcelona, Spain
[b] Department of Chemistry, P.O. Box 35, 40014, Jyväskylä, Finland
[c] Institut de Nanociència i Nanotecnologia (IN^{2}UB), Universitat de Barcelona, 08028, Barcelona, Spain

ARTICLE INFO

Article history:
Received 9 May 2019
Received in revised form
27 June 2019
Accepted 2 July 2019
Available online 5 July 2019

Keywords:
gold(I)
Aurophilicity
X-ray structure
Emission
silver(I)

ABSTRACT

The synthesis of two dinuclear ionic complexes with chemical formula $[Au(PR_3)_2][Au(C{\equiv}CC_5H_4N\text{-}4)_2]$ that contain the water soluble phosphines, PR_3, PTA (1, 3,5-triaza-7-phosphaadamantane, **1**) and DAPTA (3,7-diacetyl-1,3,7-triaza-5-phosphabicyclo[3.3.1]nonane, **2**) is herein described. The differences on their intermolecular reorganization have been analyzed and compared with the previously reported for the neutral complexes $[Au(PR_3)(C{\equiv}CC_5H_4N\text{-}4)]$. It has been evidenced that the reorganization of the ligands giving rise to the dinuclear ionic complexes produces a complete change in the properties giving rise to Au···Au intermolecular assemblies. These aurophilic contacts are the responsible for the resulting luminescence which is not displayed for the parent compounds $[Au(PR_3)_2]Cl$ and $[PPh_4][Au(C{\equiv}CC_5H_4N\text{-}4)_2]$.

Compounds **1** and **2** were made react with three different silver salts (nitrate, triflate and hexafluorophosphate) giving rise to 1:1 heterometallic assemblies with some changes both on the wavelength and emission intensity.

1. Introduction

Controllable aggregation of gold(I) compounds (complexes) is an intriguing area due to their self-assembled aggregates with particular morphologies. Synergistic aurophilic and electrostatic interactions, as well as hydrogen bonding of gold(I) compounds, can lead to the formation of fascinating supramolecular architectures with intriguing electronic, optical, and catalytic properties [1,2]. In particular, numerous gold(I) complexes possess remarkable luminescence properties with long-lived emission and sizable Stokes shifts, which turn them into promising luminescent materials for various practical applications such as solid-state vapochromic, temperature-dependent, and mechanochromic luminescent responses [3–8]. Importantly, reports have appeared on the utilization of "off–on" Au···Au interactions for solution-state sensing applications [9].

In this respect, both homo- and heteroleptic alkynyl complexes of gold(I) are at the forefront of research efforts, as these species are readily accessible, are often highly emissive, and may themselves serve as building blocks for the preparation of assemblies of yet higher complexity. This special relevance in supramolecular chemistry is based on three special characteristics: their linearity, the wide variety of coordination modes of the unsaturated bond, and the ability of gold(I) to establish metallophillic interactions [10]. The driving forces that enable self-aggregated materials stem from the ability of the smaller molecular entities to arrange spontaneously into more organized systems, but monitoring of the assembly process and comprehensive control of the final structures are often elusive [11,12] and can be analyzed based on cooperative and isodesmic models [13,14].

On the other hand, the formation of non-covalent bonding between metals (metallophilic interactions) can also be observed with other metals like silver and in heterometallic complexes like the formation of Au···Ag interactions with strength similar to that of aurophilic contacts [15].

The synthetic strategies allowing for the preparation of new types of luminescent Au(I)–Ag(I) heterometallic complexes are, nowadays, solution-based chemistry approaches, which often include the use of bridging ligands assisting the coordination of

* Corresponding author. Departament de Química Inorgànica i Orgànica, Secció de Química Inorgànica, Universitat de Barcelona, Martí i Franquès 1-11, 08028, Barcelona, Spain.
E-mail address: laura.rodriguez@qi.ub.es (L. Rodríguez).

https://doi.org/10.1016/j.jorganchem.2019.07.001
0022-328X/

different closed-shell metal centres or the direct formation of unsupported Au(I)···Ag(I) interactions [16,17]. The reaction of a neutral Au(I) complex with a silver salt gives rise to the formation of ionic heterometallic structures where the chosen counterion is observed to present a key role both in the resulting supramolecular assemblies and recorded luminescence [17–21].

Taking into consideration all these previous knowledge, in this work we have developed new ionic gold(I) complexes with general formulae $[Au(PR_3)_2][Au(C{\equiv}CC_5H_4N\text{-}4)_2]$ (PR_3 = PTA (**1**), DAPTA (**2**)). The aggregation behavior of the complexes was carefully analyzed and compared with the previously reported neutral compounds $[Au(C{\equiv}CC_5H_4N\text{-}4)(PR_3)]$ [22,23] that contain the same phosphine and 4-pyridylethynyl ligands but with different rearrangement.

Additionally, the possible formation of Au–Ag heterometallic structures has been explored in order to check how can be affecting on the resulting luminescence.

2. Results and discussion

2.1. Synthesis and characterization

The dinuclear ionic gold(I) complexes were synthesized by the reaction of $[Au(PR_3)_2]Cl$ (PR_3 = PTA, DAPTA) with $[PPh_4][Au(C{\equiv}CC_5H_4N\text{-}4)_2]$ in 1:1 ratio and in dichloromethane at room temperature for 2 h, as shown in Scheme 1:

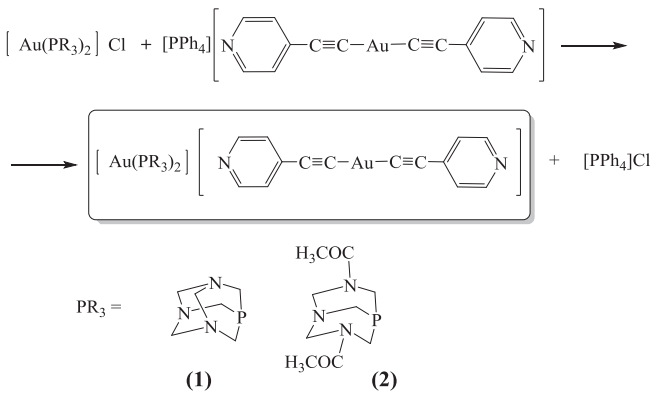

Scheme 1. Synthesis of the dinuclear ionic gold(I) complexes.

The compounds were obtained in pure form after washing with MeOH:THF. Complete removal of PPh_4Cl salt was specially challenging in the case of **2** due to their similar solubility properties in several different solvents. Previous recrystallization with methanol followed by exhaustive washing process in MeOH: THF in 1:4 was required in this case, decreasing the global yield of the reaction. Purification by column chromatography was not possible since the compound was observed to decompose.

Characterization of the complexes by ^1H and ^{31}P NMR spectroscopy, ESI-MS(+) and (−) spectrometry and IR spectroscopy evidence the correct formation of the desired products and their purity. $^{31}P\{^1H\}$ NMR display in all cases a single resonance, at −50.6 and −22.4 which are *ca.* 15 ppm downfield shifted with respect to their parent $[Au(PR_3)_2]Cl$ complexes. ^1H NMR confirms the only presence of pyridyl and PTA or DAPTA phosphines (for **1** and **2** respectively) protons (Fig. 1). The complete removal of the PPh_4Cl subproduct was also evidenced by this technique.

IR spectra display the $\nu(C{\equiv}C)$ vibration at 2098 and 2101 for **1** and **2** respectively, which is in the same region than the starting complex $(PPh_4)[Au(C{\equiv}Cpy)_2]$ since the change of the counterion is not affecting the chemical environment around the alkynyl bond. The presence of the molecular peaks recorded in all cases by ESI-MS spectrometry in positive and negative form confirms definitively the successful formation of all complexes. The molecular peaks of both cationic (m/z = 511.1 for **1** and 655.2 for **2**) and anionic counterparts (at m/z = 401.0) were detected.

Absorption and emission spectra of the complexes were recorded in $1{\cdot}10^{-5}$ M DMSO solutions at room temperature and the obtained data are summarized in Table 1. The electronic absorption spectra (Figs. 2 and S9) show intense high-energy vibronically resolved bands at *ca.* 290 nm. The intense and vibronically structured electronic absorption in the range 270–288 nm, with progression spacings of *ca.* 1900 cm^{-1}, typical of $\nu(C{\equiv}C)$ stretching frequencies in the excited state, is assigned to intraligand (IL) π-π* (C≡Cpy), as has been seen in other reported alkynyl gold(I) phosphine complexes [22–29]. This attribution is also confirmed by the

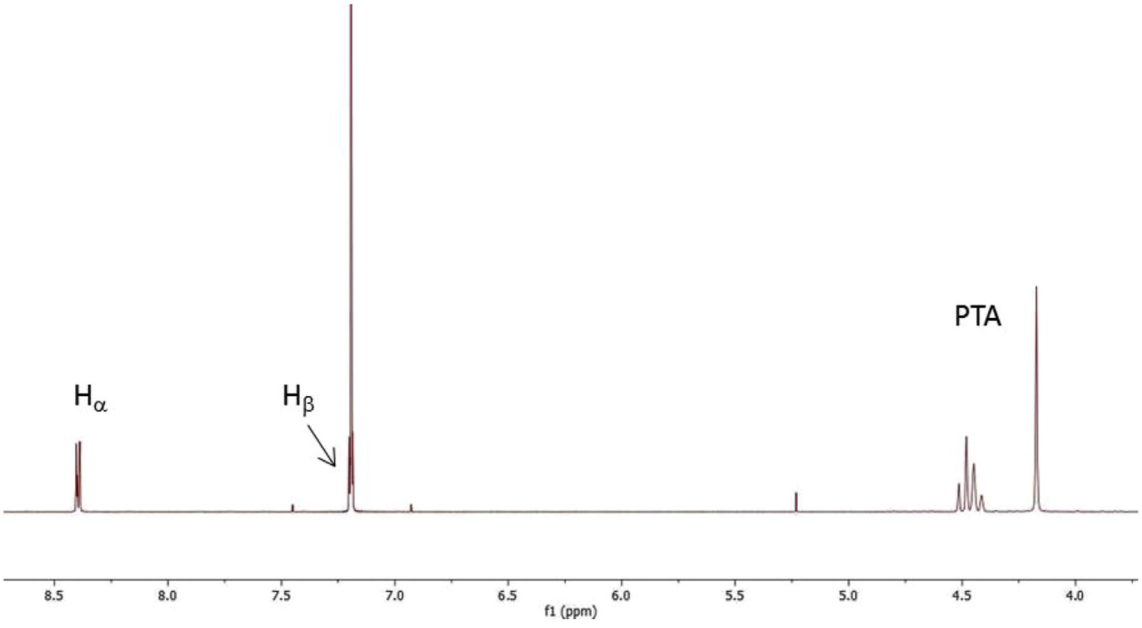

Fig. 1. ^1H NMR spectrum of **1** in $CDCl_3$.

Table 1
Absorption and emission spectral data of **1** and **2** in DMSO; $\lambda_{exc} = 300$ nm.

Compound	Absorption λ_{max} (nm) ($10^{-3}\varepsilon$ (M^{-1} cm^{-1}))	Emission λ_{max} (nm)
1	273 (41.3), (51.6), 305sh (22.7)	418, 435, 445
2	270 (38.4), 284 (51.9)	416, 437, 448

observation of excitonic perturbations due to π–π stacking in solution (ascribed by the low resolution between vibronic absorption bands) between pyridylethynyl moieties, as we previously demonstrate [24]. The higher emission band at 440 nm is assigned to ^{3}MLCT/^{3}LLCT transition [22–24,26,29–31]. The vibronic structure of these bands, and comparison with previously reported compounds containing the same chromophore [22–25], is also in agreement with the involvement of the ligands in the transition. The triplet assignment is also supported by performing emission experiments in the presence and in the absence of oxygen and applying Stern-Volmer equation (considering oxygen as quencher and DMSO as medium of the reaction). In this case, we can estimate emission lifetime values in both cases in the order of 50 μs, in agreement with phosphorescence (Fig. S13). Excitation of the powders displays in both cases a new broad band centered at 500 nm, which is more intense upon excitation the samples at 350 nm (Fig. 2 below), assigned to aggregated samples, mainly due to MMLCT transitions (see below Aggregation Section).

Excitation spectra collected at the emission maxima reproduces the absorption spectra. The lack of emission displayed by the (PPh_4)[Au(C≡Cpy)$_2$] [25] and [Au(PR_3)$_2$]Cl precursors is in agreement with a particular arrangement of the molecules in the new systems that is not present in their isolated parent compounds. This fact suggests that the observed emission may arise from intermetallic interactions between anionic and cationic part of the molecule. The presence of phosphine ligands could be also a factor that contributes to the resulting luminescence, since these ligands have been observed to favor the emissive properties in addition to improve the solubility of multinuclear species [32]. Definitive evidence was retrieved from single crystal X-ray crystal diffraction study. The good quality single crystals for **2** were successfully grown by slow evaporation of a dichloromethane solution. The X-ray structure reveals that the cationic and anionic parts of the complex are perpendicular to each other connected by short aurophilic Au–Au contact of 3.0100(5) Å. The acetylene ligands coordinated to the Au(I) centre are nearly linear with C–Au–C and C≡C–C angles of 179.6(5) and 176.2(7)°, respectively (Fig. 3). The P–Au and Au–C bond distances and angles are also in good agreement with previously reported Au(I) complexes with similar ligands [19,25,29,33–37]. The complex forms a closed packed structure without any lattice solvent molecules via a large number of weak intrermolecular interactions, such as N(py)···H, C=O···H, Au···H, H···C≡C and C–H···π (Fig. 3, Figure S11-S13), similar to previously reported gold(I) complexes [33,38].

The presence of aurophilic and other weak contacts may be maintained in solution according to absorption data (broad absorption bands and tails) while, at the same type, perfectly resolved ^{1}H NMR can be recorded, since the cross-conformation between anionic and cationic parts precludes the establishment of Au···π interactions which would hinder the observation of good signals with NMR.

2.2. Aggregation in water and water/DMSO mixtures

The aggregation of our samples in water and water/DMSO mixtures was analyzed taking into consideration the previously behavior observed for analogous gold(I) complexes containing the same ligands but with different reorganization within the chemical

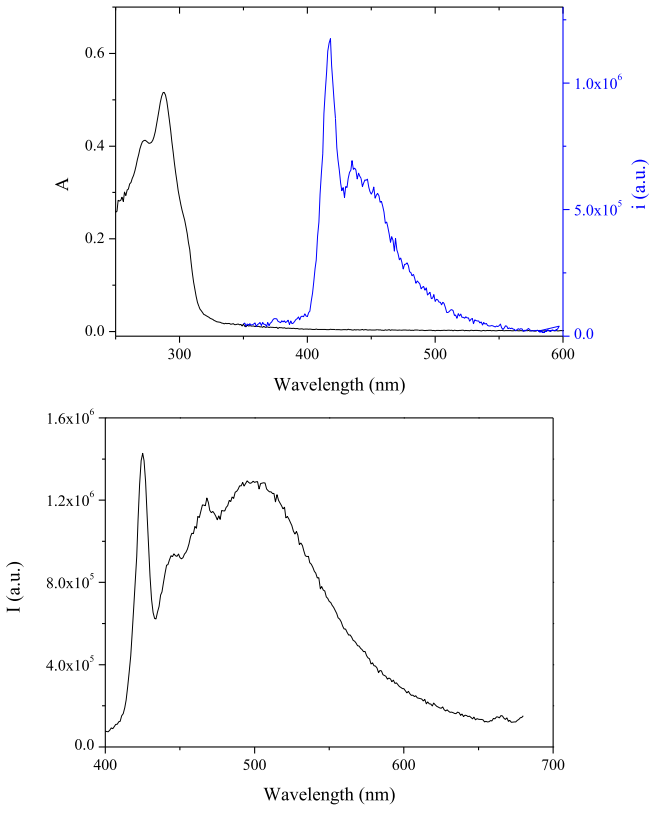

Fig. 2. Above: Absorption (black line) and emission (blue line) spectra of [Au(DAPTA)$_2$][Au(C≡CC_5H_4N-4)$_2$] (**2**) in DMSO at $1\cdot10^{-5}$ M concentration ($\lambda_{exc} = 300$ nm). Below: Emission of solid **2** upon excitation at 350 nm. (For interpretation of the references to colour in this figure legend, the reader is referred to the Web version of this article.)

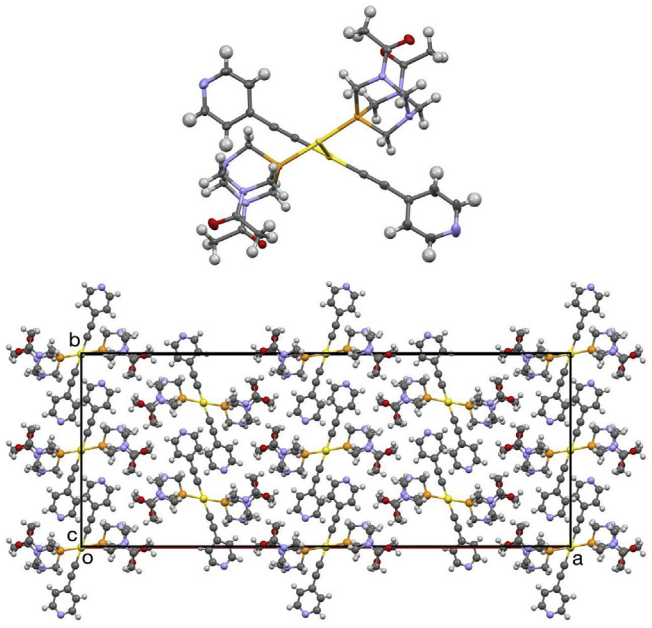

Fig. 3. X-ray crystal structure of **2** with thermal displacement parameters at 50% propability level (above) and of the packing of the molecules along the *c*-axis (below). Selected distances and angles: P–Au–P = 172.3(2)°; C≡ = 1.206(9) Å; Au–C = 1.995(6) Å; Au–P = 2.290(1) Å.

structure (neutral phosphine-Au-pyridylethynyl complexes) [14].

Absorption and emission spectra of diluted concentrations of **1** and **2** ($1\cdot10^{-5}$ M) were recorded in order to detect the initial steps of the aggregation process in DMSO:H_2O mixtures at different proportions and freshly measured. The recorded absorption spectra of **1** and **2** (Fig. 4 and Figure S14) reveal a blue shift, decrease on intensity and band broadening of the intraligand (IL) π-π* (C≡Cpy) with increasing water composition. At the same time, a lower intensity band appears around 320 nm together with an increase of the baseline in agreement with aggregates' formation [39]. This band has been assigned to a low emissive $\sigma^*_{Au-Au} \rightarrow \pi^*$ transition [26,40].

Progressive decrease of the emission was recorded with increasing water composition. This behavior was previously observed with other complexes recently reported by us [26], and can be explained due to the presence of less emissive excimers due to π–π stacking or Au-π stacking in the aggregates formed in aqueous medium.

Similar experiments were performed following changes on the increasing water contents by ^{1}H and ^{31}P NMR at different temperatures and concentrations. NMR spectra were recorded at $2\cdot10^{-4}$ M concentration in different DMSO-d_6:D_2O mixtures. It can be clearly observed that the compounds are perfectly dissolved only at higher DMSO contents (100 and 75%) while the increasing of D_2O induce a broadening of the signals (due to aggregation where the pyridyl moieties are involved) until almost disappear (Fig. 5). Some precipitation is detected from 50% D_2O contents in agreement with the lower solubility of the molecule in water at NMR concentrations.

Nevertheless, aggregation could also happen in a good solvent such as DMSO [26] where aurophilic forces may drive the intermolecular assemblies, as evidenced by the X-ray crystal structure of **2**. ^{1}H and ^{31}P NMR spectra were recorded in DMSO-d_6 solutions at different concentrations, between $2\cdot10^{-4}$ and $8\cdot10^{-4}$ M. Two different sets of H_α and H_β protons have been recorded in both cases and the corresponding variation of intensity with concentration let us assign the protons corresponding to the more aggregated structures as the more downfield shifted protons (see SI). No broadening of the peaks were recorded in this case, and this has been adscribed to Au···Au driven aggregates in DMSO (instead of Au···π that may occur in aqueous medium).

Slight upfield shift (*ca.* 0.05 ppm) of the different protons (H_α, H_β pyidyl protons and those corresponding to the phosphines) is recorded with increasing concentration, as previously observed with $PR_3AuC{\equiv}Cpy$ complexes [22,23] (Figs. S19–S20).

^{31}P NMR spectra recorded at the same concentrations range are in agreement with aggregation process. The resonance of phosphorus is slightly upfield shifted (*ca.* 0.25 ppm) with increasing concentration. Two different ^{31}P environments were recorded for **2**, as previously observed for (poly)pyridylethynyl gold(I) complexes containing the same phosphine [26], due to the possible cis-trans dynamic process of the tertiary amide groups in the phosphine within the aggregates.

For the solution-based bottom-up nanostructures, elaborated control over their morphologies and sizes requires a profound understanding of the self-assembling mechanism. Depending on the energy evolution for the self-assembling systems, there are two different types of mechanisms, namely isodesmic and cooperative mechanisms [41,42]. The cooperative mechanism begins with an energetically unfavorable nucleation step, followed by a more favorable chain-elongation stage. As a result, it avoids the existence of small oligomers, and thereby prefers to form ordered and large-sized nanostructures [13]. Based on our previous expertise that demonstrates that our complexes display first aggregation steps through vesicle type structures formation [14,35], we aim at the isodesmic model as the preferred for aggregation motif.

Variable temperature ^{1}H NMR measurements were performed at $8\cdot10^{-4}$ M concentration in DMSO–d_6 in order to use the isodesmic model to describe the thermodynamic parameters involved in the observed self-assembly. This model is based on an aggregation constant in which each monomer (M) addition to the growing chain is directed by the same equilibrium constant, K, exemplified in equations (1)–3)

$$M + M \leftrightarrow M_2 \tag{1}$$

$$M_2 + M \leftrightarrow M_3 \tag{2}$$

$$M_n + M \leftrightarrow M_{n+1} \tag{3}$$

To fit the temperature dependent ^{1}H NMR resulting from constant concentration c_0, in which K is the equilibrium constant and c_m the concentration of the monomer, molar fractions of monomer, x_m, and aggregates, x_a, can be obtained

$$x_m = \frac{c_m}{c_0} = \frac{1 + 2Kc_0 - \sqrt{1 + 4Kc_0}}{2K^2c_0^2} \tag{4}$$

$$x_a = 1 - x_m = 1 - \frac{1 + 2Kc_0 - \sqrt{1 + 4Kc_0}}{2K^2c_0^2} \tag{5}$$

In both equations the equilibrium constant K changes within the

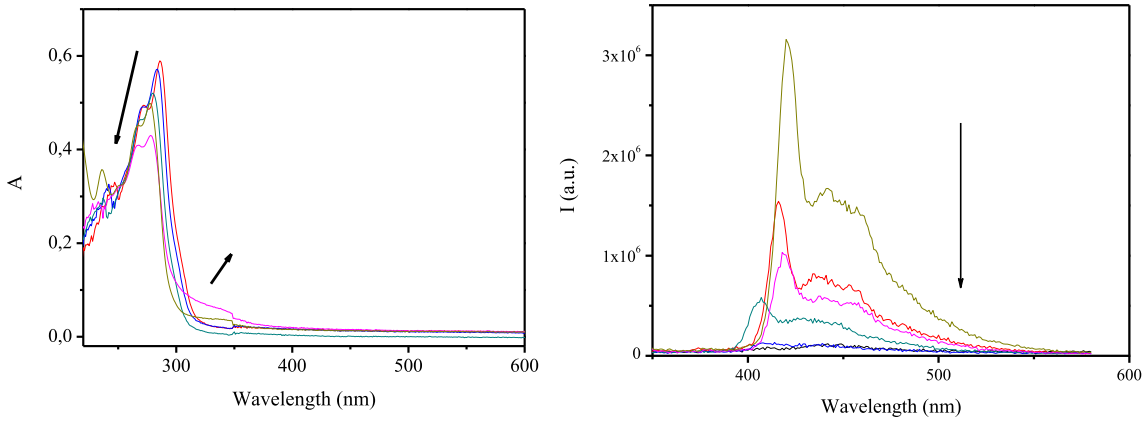

Fig. 4. Absorption (left) and emission (right) spectra of **1** at different DMSO:H_2O compositions and at $1\cdot10^{-5}$ M concentration. ($\lambda_{exc} = 300$ nm).

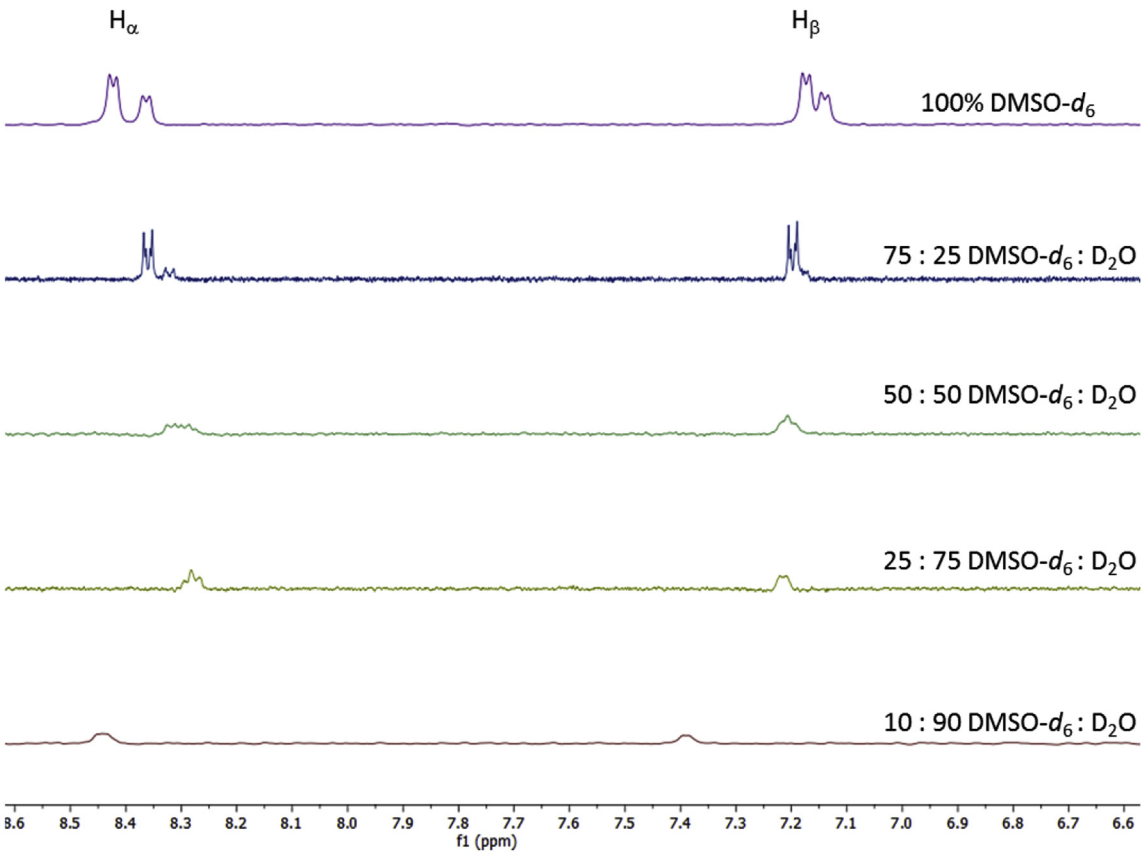

Fig. 5. ^{1}H NMR spectra (aromatic region) of **1** at different DMSO-d_6:D_2O contents at $2\cdot10^{-4}$ M.

temperature according to equation (6)

$$K = e^{-\left(\frac{\Delta G}{RT}\right)} \tag{6}$$

where ΔG is the Gibbs free energy, R is the gas constant and T is the temperature. Since the temperature range of the experiments is small and ΔG is Temperature dependent, more suitable equation (7) is used to determine the thermodynamic constants of the self-assembly

$$K = e^{-\left[\left(\frac{\Delta H}{RT}\right)+\left(\frac{\Delta S}{R}\right)\right]} \tag{7}$$

where ΔH is the enthalpy and ΔS is the entropy.

The temper ature dependent ^{1}H NMR data were fitted in equations (4) and (5). Plots of x_{mon} and x_{aggreg} for both **1** and **2** complexes (Fig. S23) show that, as expected [14], the formation of aggregates is more favored at low temperatures.

The results displayed in Table 2 reveal that the entropy drives the aggregation process, which can arise from the release of solvent molecules upon interaction between molecules. This is the main difference with respect to their parent neutral compounds where a negative enthalpy contributions was observed [14]. In the previous case, a reorganization of individual molecules was the driving force of the aggregation upon formation of different type of intermolecular interactions. On the contrary, compounds **1** and **2** already present intermolecular contacts with interactions between the positive and negative counterparts throught Au···Au interactions. For this reason, herein we expect higher contribution of the entropic factor.

Table 2
Enthalpy, Entropy, Gibbs Free Energy and equilibrium constant K at 298 K for compounds **1** and **2** at $8\cdot10^{-4}$ M concentration in DMSO. The error was estimated from the differences in molar fractions determined against the total area of the pyridyl protons and against the area of an internal reference.

	ΔH (kJ/mol)	ΔS (J/mol·K)	ΔG^{298} (kJ/mol)	K^{298}
1	6 ± 0.5	75 ± 1	−17 ± 1	815
2	12 ± 1	81 ± 2	−12 ± 0.5	150

The Gibbs free energy for a single step aggregation obtained from the VT ^{1}H NMR data is slightly lower than the previously recorded for the neutral complex in water due to the lower contribution of the enthalpic factor, since some aggregation seems to be present in all cases.

2.3. Modulation of absorption and emission by interaction with silver salts

Absorption and emission spectra of $1\cdot10^{-5}$ M DMSO solutions of **1** and **2** were recorded upon addition of different amounts of three different silver salts in order to find out the possible formation of heterometallic compounds and the effect on the resulting luminescence. As previously observed [19], counterions can have a direct effect on the resulting heterometallic structures and for this reason, nitrate, hexafluorophosphate and triflate silver salts were used.

Absorption and emission titrations indicates in all cases the formation of a 1:1 heterometallic complex. It is observed a progressive decrease on the absorption band at 298 nm together with the appearance of a new band at *ca.* 330 nm before the one

equivalent that then decreases to give rise to a new band at *ca.* 315 nm. Emission spectra changes recorded upon excitation the samples both at 295 nm and 330 nm are in agreement with the presence of a more emissive intermediate species before one equivalent and then emission is stabilized at 1:1 Au:Ag heterometallic system (Figs. S24–S35). That means that the formation of 1:1 heterometallic structures are the thermodynamic more stable complexes while intermediate structures with different stoichiometry can be also detected in the process.

Changes on the emission wavelength and intensities are summarized in Fig. 6. Thus, in the case of **1** the recorded emission maxima are blue shifted 4 and 7 nm in the case of triflate and nitrate anions respectively and 9 nm for both anions in the case of **2**. No significant changes were recorded in the presence of $AgPF_6$ salt (Fig. 7).

Additionally, no changes on emission intensity were recorded for nitrate derivatives in both cases, while emission intensity increases *ca.* 2- and 3.4 fold for triflate (for **1** and **2** respectively) and decreases to the half for **1**·PF_6 derivative (Figs. S36–37). Obviously, these are not absolute values of intensity since they are not based on quantum yields measurements.

Thus, it seems that the strongest interaction with the counterion is observed for the O-coordinating anions (NO_3^- and $OSO_2CF_3^-$) while no significant interaction is expected (according to changes on emission wavelength) for the bulkier and spherical PF_6^- anion. The difference on emission intensity in both heterometallic PF_6 complexes (with lower and higher emission intensity with respect to homometallic complexes) must be ascribed to the bulkiness of the DAPTA phosphine (**2**). ^{1}H NMR spectra recorded in the presence of one equivalent of the different silver salts support this evidence (Figs. S38 and S39), since nitrate and triflate heterometallic complexes display broadening pyridyl protons with different environments, typical for aggregates' formation [14] together with a small downfield shift of ca. 0.05–0.2 ppm. On the contrary, although less significant variations have been recorded for the corresponding PF_6 derivatives, pyridyl protons become more defined in both **1**·PF_6 and **2**·PF_6 derivatives suggesting a disaggregation process where the aromatic heterocycle is directly involved.

In depth characterization must be carried out for these new systems (mainly, if possible, growing single crystals suitable for X-ray diffraction resolution) in order to find out the resulting structure of the heterometallic systems. Nevertheless, taking into consideration these results, we can affirm that absorption and emission spectroscopy are relevant characterization techniques to identify the formation of 1:1 heterometallic structures in all cases. The resulting intensity and the emission wavelength of the new systems can be modulated by the easy interaction with a silver salt. Mainly, the adequate choice of the counteranion is the key point in the resulting luminescent properties of the heterometallic systems.

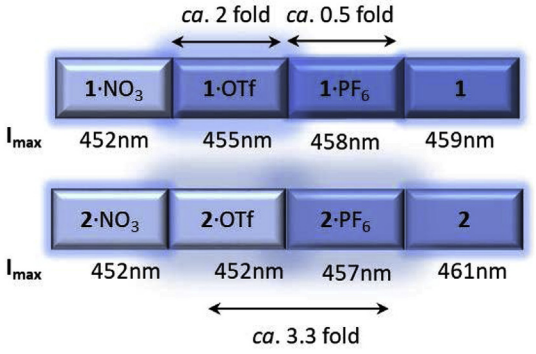

Fig. 6. Counteranion dependence scheme of the recorded changes on the shift and emission intensity upon the formation of heterometallic complexes.

3. Conclusions

The dinuclear character of the ionic complexes $[Au(PR_3)_2][Au(C{\equiv}CC_5H_4N\text{-}4)_2]$ (PR_3 = PTA (**1**) and DAPTA (**2**)) induces aurophilic structures by cation···anion interactions, as shown by single crystal X-ray crystal diffraction.

Absorption and emission studies at different compositions of DMSO/H_2O suggested a formation of aggregates at low concentrations (*ca.* 10^{-5}) in all cases and more favored with increasing water composition. The aqueous aggregates induce a quenching effect on the supramolecular assemblies. ^{1}H and ^{31}P NMR studies support these observations.

The analysis of the ^{1}H NMR data fitted with isodesmic model indicates that, as a difference with the neutral parent compounds $[Au(PR_3)(C{\equiv}CC_5H_4N\text{-}4)]$, aggregation is driven by entropic effects.

Absorption and emission titrations of DMSO solutions of **1** and **2** with different silver salts (nitrate, triflate and hexafluorophosphate) indicates the formation of 1:1 heterometallic Au/Ag complexes. Anions are expected to have a direct effect on the assemblies since different behavior is observed (enhancement or quenching of the emission).

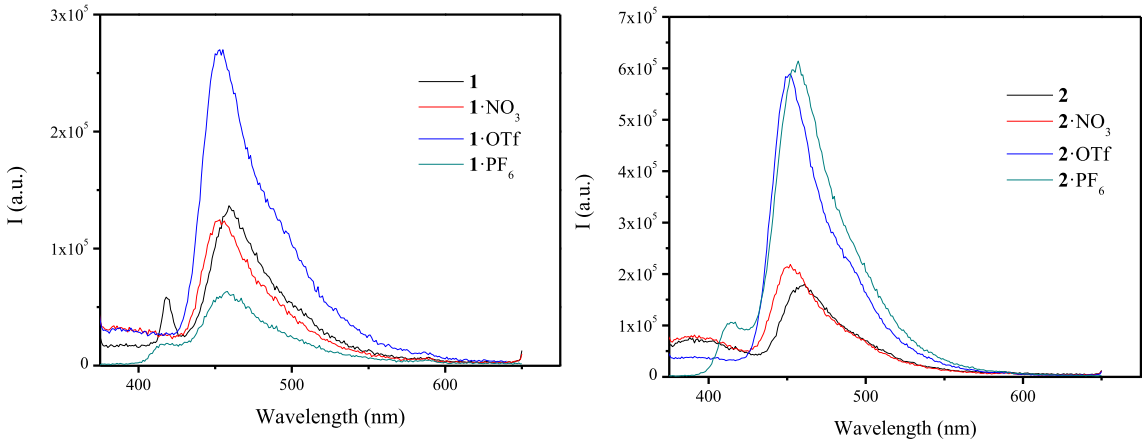

Fig. 7. Normalized emission spectra of **1** and **2** and corresponding heterometallic complexes. (λ_{exc} = 330 nm).

4. Experimental section

4.1. General procedures

All manipulations have been performed under prepurified N_2 using standard Schlenk techniques. All solvents have been distilled from appropriated drying agents. Commercial reagents Ammonium hydroxide (Aldrich), Tetraphenylphosphonium chloride (Aldrich, 98%), Thallium(I) acetylacetonate (Aldrich), 1,3,5-triaza-7-phosphatricyclo[3.3.1.13.7]decane (PTA, Aldrich 97%), 3,7-diacetyl-1,3,7-triaza-5-phosphabicyclo[3.3.1]nonane (DAPTA, Aldrich 97%), were used as received. Prior to use, solvents were distilled from drying agents except MeOH and ACN, which were purged. Literature method was used to prepare $[Au(PTA)_2]Cl$ [43] and $[PPh_4][Au(C{\equiv}CC_5H_4N\text{-}4)_2]$ [25].

4.2. Physical measurements

Infrared spectra were measured using a FT-IR 520 Nicolet Spectrophotometer. ^1H NMR (δ(TMS) = 0.0 ppm) and $^{31}P\{^1H\}$-NMR spectra were measured with a Varian Mercury 400 MHz and a Bruker 400 MHz Avance III spectrometers. ElectroSpray-Mass spectra (+and -) were recorded using a Fision VG Quatro spectrometer. Absorption spectra were recorded on a Varian Cary 100 Scan UV-spectrophotometer and emission spectra were recorded using a Horiba-Jobin-Yvon iHR320 spectrofluorimeter. Dynamic light scattering measurements were carried out by using MALVERN Zetasizer Nano ZS instrument at 173° scattering angle and 25 °C.

4.3. X-ray structure determination

The crystal data and experimental details for the data collection are given in Table S1. The single crystal X-ray data for **2** were collected using a Rigaku-Oxford Diffraction SuperNova dual-source diffractometer with an Atlas CCD detector using mirror-monochromated Cu-Kα ($\lambda = 1.54184$ Å) radiation. The data collection and reduction was performed using the program CrysAlisPro [44] and Gaussian face index absorption correction method was applied [44]. The structure was solved with direct methods (*SHELXT*) [45a] and refined by full-matrix least squares on F^2 using the *OLEX2* software [46], which utilizes the *SHELXL*-2014 module [45b]. CCDC-1914062 contains the supplementary crystallographic data for this paper. These data can be obtained free of charge from The Cambridge Crystallographic Data Centre via www.ccdc.cam.ac.uk/data_request/cif.

4.4. NMR measurements in DMSO and H_2O

Samples were prepared from 1a by diluting 1.0 mg of the compound in 1:0, 3:1, 1:1, 1:3 and 0:1 v/v mixtures of DMSO and double-distilled water. Some solid remained in the NMR tube although it was mixed in ultrasound (Ultrasons P Selecta).

4.5. Absorption measurements

To prepare two stock solutions of **1** and **2**, 0.60 mg of each compound was dissolved in 25.0 ml of double-distilled water and DMSO. Then, the 10^{-5} M sample solutions in 1:0, (9:1 only for 1b), 3:1, 1:1, 1:3, 1:9 and 0:1 v/v mixtures of DMSO:H_2O were prepared from the stock solution. All measurements were made after the sample preparation as the aggregation of the compounds can vary with time. In both analyses, volumes smaller than 25 ml were measured with labopette® (Hirschmann Laborgeräte) micropipettes. The experiments were repeated three times in order to have more accurate results, due to the low solubility of the compounds in water.

4.6. Synthesis of the complexes

4.6.1. Synthesis of $[Au(DAPTA)_2]Cl$

Solid DAPTA (0.071 g, 0.31 mmol) was added to a suspension of Au(tht)Cl (0.099 g, 0.31 mmol) in dry ACN (7.0 ml) at room temperature under nitrogen atmosphere. After 2 h of stirring, a second fraction of DAPTA (0.072 g, 0.31 mmol) was added at once and stirred for additional 2 h. The resulting white suspension was concentrated in half volume and diethylether (10.0 ml) was added to precipitate a white product which was filtered and washed with cold diethylether (2 × 2.0 ml) to give the resulting $[Au(DAPTA)_2]Cl$ as a white powder in pure form (0.19 g, 87%). ^1H NMR (400 MHz, $CDCl_3$): δ_H 5.81 (2H, d, $J = 16.0$ Hz, N–CH_2–N), 5.62 (2H, dd, $J = 16.0$, 8.0 Hz, N–CH_2–P), 4.98 (2H, d, $J = 12.0$ Hz, N–CH_2–N), 4.60–4.68 (4H, m, N–CH_2–N and N–CH_2–P), 4.15 (2H, ddd, $J = 15.6$, 4.8, 2.8 Hz, N–CH_2–P), 4.07 (2H, d, $J = 16.0$ Hz, N–CH_2–N), 3.86 (4H, s, N–CH_2–P), 3.53 (2H, ddd, $J = 16.6$, 5.6, 2.4 Hz, N–CH_2–P) and 2.12 (12H, s, CO–CH_3) ppm. $^{31}P\{^1H\}$-NMR ($CDCl_3$, 400 MHz): δ −36.6 (s, 1P). IR (KBr, cm^{-1}): ν (C═O) 1649.

4.6.2. Synthesis of $[Au(PTA)_2][Au(C{\equiv}CC_5H_4N\text{-}4)_2]$ (**1**)

$[PPh_4][Au(C{\equiv}CC_5H_4N\text{-}4)_2]$ (0.073 g, 0.099 mmol) was added to a suspension of $[Au(PTA)_2]Cl$ (0.054 g, 0.099 mol) in DCM (10.0 ml) at room temperature under an atmosphere of nitrogen. After stirring for 2 h a white suspension was concentrated and DEE (25.0 ml) added to precipitate the product. The mixture was left in a fridge for 12 h. A white precipitate was filtrated with cannula and washed with cold DEE (2 × 3.0 ml). The product was dried under vacuum and purified by diluting in DCM (10.0 ml), dried and diluted in 4:3 THF:MeOH (9.0 ml). White suspension was left in a fridge for 3 h. The product was filtrated with cannula, washed with cold MeOH (2.0 ml) and dried in vacuum to give $[Au(DAPTA)_2][Au(C{\equiv}CC_5H_4N\text{-}4)_2]$ as a white solid (0.068 g, 76%). ^1H NMR (400 MHz, $CDCl_3$): δ_H 8.47 (4H, ABq, $J_{AB} = 1.6$ Hz, N–CH_α–N), 7.27 (4H, ABq, $J_{AB} = 1.6$ Hz, N–CH_β–N), 4.53 (12H, dd, $J = 24.0$, 12.0, 16.0 Hz, N–CH_2–N) and 4.24 (12H, s, N–CH_2–P) ppm. $^{31}P\{^1H\}$-NMR ($CDCl_3$, 400 MHz): δ −50.6 (s, 1P). IR (KBr, cm^{-1}): ν (C═C) 1587, 970, ν (P–C) 1099, ν (C≡C) 2098, ν (N–C) 1243. ESI-MS(+) *m/z*: 529.1301 ($[M+H_2O]^+$, calc: 529.1309). ESI-MS (−) *m/z*: 401.0364 ($[M]^-$, calc: 401.0353). Anal. Calc.: C, 34.22; H, 3.53; N, 12.28. Anal. Found: C, 34.28; H, 3.57; N, 12.32.

4.6.3. Synthesis of $[Au(DAPTA)_2][Au(C{\equiv}CC_5H_4N\text{-}4)_2]$ (**2**)

$[PPh_4][Au(C{\equiv}CC_5H_4N\text{-}4)_2]$ (0.053 g, 0.071 mmol) was added to a suspension of $[Au(DAPTA)_2]Cl$ (0.068 g, 0.053 mol) in DCM (25.0 ml) at room temperature under an atmosphere of nitrogen. After stirring for 2 h an orange solution was concentrated and diethylether (25.0 ml) added to precipitate the product. A yellow product was filtrated with cannula and washed with cold diethylether (2 × 3.0 ml). The product was recrystallized from 4:1 THF:MeOH (9.0 ml) to give $[Au(DAPTA)_2][Au(C{\equiv}CC_5H_4N\text{-}4)_2]$ as a yellow solid (0.010 g, 14%). ^1H NMR (400 MHz, $CDCl_3$): δ_H 8.47 (4H, ABq, $J_{AB} = 1.6$ Hz, N–CH_α–N), 7.28 (4H, ABq, $J_{AB} = 1.6$ Hz, N–CH_β–N) 5.82 (2H, d, $J = 12.0$ Hz, N–CH2–N), 5.65 (2H, dd, $J = 16.0$, 4.0 Hz, N–CH2–P), 4.98 (2H, d, $J = 16.0$ Hz, N–CH_2–N), 4.59–4.68 (4H, m, N–CH2–N and N–CH_2–P), 4.05–4.13 (4H, m, N–CH_2–P and N–CH_2–N), 3.83 (4H, s, N–CH_2–P), 3.49 (2H, dt, J = 16.0, 4.0, Hz, N–CH_2–P) and 2.12 (12H, s, CO–CH_3) ppm. $^{31}P\{^1H\}$-NMR ($CDCl_3$, 400 MHz): δ −22.4 (s, 1P). IR (KBr, cm^{-1}): ν (C═C) 1588, ν (C═O) 1636, ν (C≡C) 2101 and ν (N–C) 1335. ESI-MS (+) *m/z*: 655.1612 ($[M]^+$, calc: 655.1626). ESI-MS (−) *m/z*: 401.0359 ($[M]^-$, calc: 401.0353). Anal. Calc.: C, 36.38; H, 3.82; N, 10.61. Anal. Found: C, 36.44; H, 3.86; N, 10.57.

Acknowledgements

The authors are grateful to the Ministry of Economy, Industry and Competitiveness of Spain (AEI/FEDER, UE Project CTQ2016-76120-P). The support and sponsorship provided by COST Action CM1402 is also acknowledged. N.S. is also indebted to Erasmus exchange mobility Program. Dr Toni Mäkelä is thanked for the data collection and preliminary structure solution of 2.

Appendix A. Supplementary data

Supplementary data to this article can be found online at https://doi.org/10.1016/j.jorganchem.2019.07.001.

References

[1] E.R.T. Tiekink, Coord. Chem. Rev. 275 (2014) 130.
[2] Y.-T. Tseng, H.-Y. Chang, S.G. Harroun, C.-W. Wu, S.-C. Wei, Z. Yuan, H.-L. Chou, C.-H. Chen, C.-C. Huang, H.-T. Chang, Anal. Chem. 90 (2018) 7283.
[3] R. Kawano, O. Younis, A. Ando, Y. Rokusha, S. Yamada, O. Tsutsumi, Chem. Lett. 45 (2016) 66.
[4] S. Yamada, S. Yamaguchi, O. Tsutsumi, J. Mater. Chem. C 5 (2017) 7977.
[5] P. Ai, M. Mauro, C. Gourlaouen, S. Carrara, L. De Cola, Y. Tobon, U. Giovanella, C. Botta, A.A. Danopoulos, P. Braunstein, Inorg. Chem. 55 (2016) 8527.
[6] J.C. Lima, L. Rodríguez, Chem. Soc. Rev. 40 (2011) 5442.
[7] P. Ai, M. Mauro, A.A. Danopoulos, A. Muñoz-Castro, P. Braunstein, J. Phys. Chem. C 123 (2019) 915.
[8] I.O. Koshevoy, Y.-C. Chang, Y.-A. Chen, A.J. Karttunen, E.V. Grachova, S.P. Tunik, J. Janis, T.A. Pakkanen, P.-T. Chou, Organometallics 33 (2014) 2363.
[9] A.A. Penney, G.L. Starova, E.V. Grachova, V.V. Sizov, M.A. Kinzhalov, S.P. Tunik, Inorg. Chem. 56 (2017) 14771.
[10] H. Schmidbaur, A. Schier, Chem. Soc. Rev. 41 (2012) 370.
[11] A. Aliprandi, M. Mauro, L. De Cola, Nat. Chem. 8 (2016) 10.
[12] K. Jie, Y. Zhou, Y. Yao, B. Shi, F. Huang, J. Am. Chem. Soc. 137 (2015) 10472.
[13] J. Chen, Z. Zhang, C. Wang, Z. Gao, Z. Gao, F. Wang, Chem. Commun. 53 (2017) 11552.
[14] R. Gavara, E. Aguiló, C. Fonseca Guerra, L. Rodríguez, J.C. Lima, Inorg. Chem. 54 (2015) 5195.
[15] J.M. López-de-Luzuriaga, M. Monge, M.E. Olmos, D. Pascual, Organometallics 34 (2015) 3029.
[16] J.M. López de Luzuriaga, M. Monge, M.E. Olmos, J. Quintana, M. Rodríguez-Castillo, Dalton Trans. 47 (2018) 3231.
[17] N. Savjani, L.A. Wilkinson, D.L. Hughes, M. Schormann, M. Bochmann, Organometallics 31 (2012) 7600.
[18] T.H.T. Hsu, J.J. Naidu, B.-J. Yang, M.-Y. Jang, I.J.B. Lin, Inorg. Chem. 51 (2012) 98.
[19] R. Gavara, A. Pinto, R. Donamaría, M.E. Olmos, J.M. López de Luzuriaga, L. Rodríguez, Inorg. Chem. 56 (2017) 11946.
[20] D. Fernández, M.I. García-Seijo, M. Bardají, A. Laguna, M.E. García-Fernández, Dalton Trans. (2008) 2633.
[21] M.C. Blanco, J. Cámara, M.C. Gimeno, A. Laguna, S.L. James, M.C. Lagunas, M.D. Villacampa, Angew. Chem. Int. Ed. 51 (2012) 9777.
[22] E. Aguiló, R. Gavara, J.C. Lima, J. Llorca, L. Rodríguez, J. Mater. Chem. C 1 (2013) 5538.
[23] R. Gavara, J. Llorca, J.C. Lima, L. Rodríguez, Chem. Commun. 49 (2013) 72.
[24] M. Ferrer, A. Gutiérrez, L. Rodríguez, O. Rossell, J.C. Lima, M. Font-Bardia, X. Solans, Eur. J. Inorg. Chem. (2008) 2899.
[25] M. Ferrer, L. Rodriguez, O. Rossell, F. Pina, J.C. Lima, M. Font-Bardia, X. Solans, J. Organomet. Chem. 678 (2003) 82.
[26] E. Aguiló, A.J. Moro, R. Gavara, I. Alfonso, Y. Pérez, F. Zaccaria, C. Fonseca Guerra, M. Malfois, C. Baucells, M. Ferrer, J.C. Lima, L. Rodríguez, Inorg. Chem. 57 (2018) 1017.
[27] M. Ferrer, L. Giménez, A. Gutiérrez, J.C. Lima, M. Martínez, L. Rodríguez, A. Martín, R. Puttreddy, K. Rissanen, Dalton Trans. 46 (2017) 13920.
[28] R. Gavara, J.C. Lima, L. Rodríguez, Photochem. Photobiol. Sci. 15 (2016) 635.
[29] M.C. Blanco, J. Camara, V. Fernández-Moreira, A. Laguna, M.C. Gimeno, Eur. J. Inorg. Chem. (2018) 2762.
[30] E. Aguiló, A.J. Moro, M. Outis, J. Pina, D. Sarmento, J.S. Seixas de Melo, L. Rodríguez, J.C. Lima, Inorg. Chem. 57 (2018) 13423.
[31] M.C. Blanco, J. Camara, M.C. Gimeno, P.G. Jones, A. Laguna, J.M. Lopez-de-Luzuriaga, M.E. Olmos, M.D. Villacampa, Organometallics 31 (2012) 2597.
[32] V. Fernandez-Moreira, J. Camara, E.S. Smirnova, I.O. Koshevoy, A. Laguna, S.P. Tunik, M.C. Blanco, M.C. Gimeno, Organometallics 35 (2016) 1141.
[33] N. Svahn, A.J. Moro, C. Roma-Rodrigues, R. Puttreddy, K. Rissanen, P.V. Baptista, A.R. Fernandes, J.C. Lima, L. Rodríguez, Chem. Eur J. 24 (2018) 14654.
[34] E. García-Moreno, S. Gascón, M.J. Rodriguez-Yoldi, E. Cerrada, M. Laguna, Organometallics 32 (2013) 3710.
[35] A.J. Moro, B. Rome, E. Aguiló, J. Arcau, R. Puttreddy, K. Rissanen, J.C. Lima, L. Rodríguez, Org. Biomol. Chem. 13 (2015) 2026.
[36] J. Arcau, V. Andermark, E. Aguiló, A. Gandioso, A. Moro, M. Cetina, J.C. Lima, K. Rissanen, I. Ott, L. Rodríguez, Dalton Trans. 43 (2014) 4426.
[37] M. Jin, T.S. Chung, T. Seki, H. Ito, M.A. Garcia-Garibay, J. Am. Chem. Soc. 139 (2017) 18115.
[38] D.-A. Rosca, J.A. Wright, M. Bochmann, Dalton Trans. 44 (2015) 20785.
[39] A. Pinto, N. Svahn, J.C. Lima, L. Rodríguez, Dalton Trans. 46 (2017) 11125.
[40] L. Rodríguez, M. Ferrer, R. Crehuet, J. Anglada, J.C. Lima, Inorg. Chem. 51 (2012) 7636.
[41] T.F.A. De Greef, M.J.M. Smulders, M. Wolffs, A.P.H.J. Schenning, R.P. Sijbesma, E.W. Meijer, Chem. Rev. 109 (2009) 5687.
[42] C. Rest, R. Kandanelli, G. Fernández, Chem. Soc. Rev. 44 (2015) 2543.
[43] Z. Assefa, J.M. Forward, T.A. Grant, R.J. Staples, B.E. Hanson, A.A. Mohamed, J.P. Fackler, J. Inorg. Chim. Acta 352 (2003) 31.
[44] Rigaku Oxford Diffraction, CrysAlisPro Version, vol. 38, 2018, p. 46.
[45] (a) G.M. Sheldrick, Acta Crystallogr. A71 (2015) 3–8;
(b) G.M. Sheldrick, Acta Crystallogr. C71 (2015) 3–8.
[46] O.V. Dolomanov, L.J. Bourhis, R.J. Gildea, J.A.K. Howard, H.J. Puschmann, J. Appl. Crystallogr. 42 (2009) 339–341.